PCCP

ROYAL SOCIETY OF CHEMISTRY

PAPER

View Article Online
View Journal | View Issue

Cite this: *Phys. Chem. Chem. Phys.*, 2023, **25**, 5459

Observation of slow magnetic relaxation phenomena in spatially isolated π-radical ions†

Shohei Koyama, *[a] Kazunobu Sato,[b] Masahiro Yamashita, [ac] Ryota Sakamoto[a] and Hiroaki Iguchi *[d]

Received 26th December 2022,
Accepted 14th January 2023

DOI: 10.1039/d2cp06026d

rsc.li/pccp

The use of molecular spins as quantum bits is fascinating because it offers a wide range of strategies through chemical modifications. In this regard, it is very interesting to search for organic radical ions that have small spin–orbit coupling values. On the other hand, the feature of the magnetic relaxation of π-organic radical ions is rarely exploited due to the difficulty of spin dilution, and π-stacking interaction. In this study, we focus on *N*,*N*′,*N*″-tris(2,6-dimethylphenyl)benzenetriimide (BTI-xy), where three xylene moieties connected to the imide groups cover the π-plane of the BTI core. As a result, BTI-xy radical anions without π-stacking interaction were obtained. This led to the slow magnetization relaxation, which is reported for the first time in organic radicals. Furthermore, the relaxation times in a solution state revealed the importance of spin interaction.

Introduction

Quantum bits (qubits) are the basic units of quantum information, which can possess quantum superposition. The manipulation and observation of qubits provide novel applications, such as quantum information processing[1] and quantum sensors.[2] To realize these exceptional functions, photons,[3] trapped ions,[4] nuclear spins,[5] and superconducting quantum circuit,[6] *etc.* have been proposed as candidates for a qubit. Among them, molecular spin-based qubits[7] which utilize the superposition of up-spin and down-spin states are interesting because of their remarkable advantages over other qubit materials, such as the ability to address electronic states of single molecules by a combination of electron spin resonance (ESR) and scanning tunneling microscopy (STM)[8] and to conduct research through chemical modification.[9] For a comprehensive understanding and development of molecule-based quantum technologies, it is important to achieve a robust spin state, which is characterized by a spin–lattice relaxation time (T_1), and a phase relaxation time (T_2). So far, S = 1/2 spins of polynuclear metal complexes,[10] V^{4+} complexes,[11] and Cu^{2+} complexes[12] have been mainly examined with pulsed ESR, alternating current (ac) magnetic susceptibility measurements, and calculation methods as a playground of molecule-based qubits, showing the importance of spin–orbit coupling, vibrational modes, and nuclear spins in the system.

On the other hand, the study on the magnetic relaxation behavior in S = 1/2 organic radicals is very promising because of a wide range of research development by chemical modification and a small spin–orbit interaction that suppresses spin–lattice relaxation. There have been several reports focusing on magnetic relaxation behaviors as well as some attempts at qubits on radicals.[13] In particular, the manipulation of light-induced spin,[13f] the phase relaxation time of more than 10 μs in diluted solutions of triarylmethyl radicals,[13e] and the implementation of quantum gates in radicals[13g] are attractive results to highlight the properties of radicals. On the other hand, redox-active π-radical ions offer a variety of possibilities for molecular qubit research not only because numerous molecular skeletons have been proposed in the field of molecular conductors and organic semiconductors,[14] but also because they can easily insert or remove electrons to switch spin states on electrodes and STM substrates.[15] Such a switching behavior has been pointed out to be important for quantum-gate manipulation between multiple qubits because it can be assumed as switching of entanglement.[16] Moreover, the rigidity of π-planes could be applied to scalable architectures such as metal–organic frameworks (MOFs).[11h,12f] Hence, π-radical ions are expected to occupy an important position in the broad study of molecular qubits. However, there have been few studies of π-radical ions aiming at longer magnetic relaxation times. This can be explained by the strong π-stacking interaction between π-radical molecules

[a] *Department of Chemistry, Graduate School of Science, Tohoku University, 6-3 Aramaki-Aza-Aoba, Aoba-ku, Sendai, 980-8578, Japan. E-mail: shohei.koyama.t3@dc.tohoku.ac.jp*
[b] *Department of Chemistry, Graduate School of Science, Osaka Metropolitan University, 3-3-138 Sugimoto, Sumiyoshi-ku, Osaka 558-8585, Japan*
[c] *School of Materials Science and Engineering, Nankai University, Tianjin 300350, P. R. China*
[d] *Department of Materials Chemistry, Graduate School of Engineering, Nagoya University, Furo-cho, Chikusa-ku, Nagoya 464-8603, Japan. E-mail: hiroaki.iguchi@chembio.nagoya-u.ac.jp*

† Electronic supplementary information (ESI) available: Crystallographic data, magnetic susceptibility, and ESR spectra. CCDC 2205572 (BTI-Xy•Toluene) 2205573 (**$CoCp_2$BTI-xy**) and 2205666 (**$CoCp^*_2$BTI-xy**). For ESI and crystallographic data in CIF or other electronic format see DOI: https://doi.org/10.1039/d2cp06026d

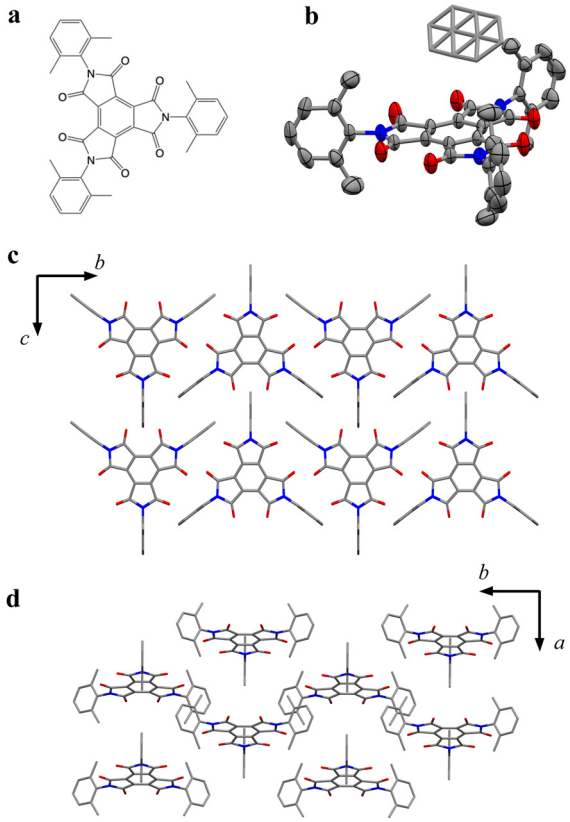

Fig. 1 (a) Chemical structure of BTI-xy. (b) Crystal structure of BTI-xy• toluene with the thermal ellipsoid plot. Disordered toluene is depicted by capped sticks. (c and d) Crystal packing structure of BTI-xy• toluene along *a* axis (c), and *c* axis (d). Toluene in (c and d) and hydrogen atoms are omitted for clarity. Purple, Co; red, O; grey, C; and blue, N.

which promotes spin–phonon coupling,[13i] and by the fact that magnetic dilution is difficult in organic ionic crystals.

Here, to highlight π-radical ions as promising candidates of a qubit, we demonstrate the magnetic relaxation behavior of π-organic radical ions where π-stacking interactions were suppressed. We focused on benzenetriimide molecules (BTIs), whose properties and structures as π-radical anions have been recently reported.[17] Specifically, we newly synthesized *N*,*N*′,*N*″-tris(2,6-dimethylphenyl)-benzenetriimide (BTI-xy), which has three xylene moieties at the imide-nitrogen sites. In this molecule, the interaction between π-organic radical molecules can be inhibited by the xylene moiety (Fig. 1a), and thus it is expected that the isolation of π-radical cores in the crystal structure occurs. In fact, two radical anion salts of BTI-xy made by reduction using cobaltocene ($CoCp_2$) or decamethylcobaltocene ($CoCp^*_2$) have no π-stacking interaction between neighboring π-radical cores. This crystal structure allows us to investigate the ac susceptibility and to measure for the first time the slow magnetic relaxation behavior of π-radicals in a crystalline state. We also measured T_1 and T_2 by pulsed ESR measurements in the solution state, and then we discussed the magnetic relaxation behaviors of π-radical ions.

Results

Structural characterization

BTI-xy was newly synthesized by following the reported method with some modifications.[17,18] Single crystals of BTI-xy• toluene were obtained by thermal recrystallization from toluene. Its crystal structure is shown in Fig. 1. BTI-xy with disordered toluene crystallizes in a monoclinic system. It is confirmed that the methyl groups of the xylene moieties cover the π-plane of the BTI molecule, inhibiting the π–π interaction between the BTI-xy molecules. In crystal structures of other BTIs, π–π interactions have been observed, suggesting that the absence of π–π interaction is due to the steric hindrance of the xylene moiety.[16] The cyclic voltammogram of BTI-xy showed redox peaks at −0.97 V, −1.69 V, and −2.53 V *vs.* Fc/Fc^+, which is similar to other BTI derivatives (Fig. S1, ESI†).[17,18] Since the potential of the first redox wave is low enough to be reduced with $CoCp_2$ and $CoCp^*_2$,[19] **$CoCp_2$BTI-xy** (**1**) and **$CoCp^*_2$BTI-xy** (**2**) were obtained by adding $CoCp_2$ and $CoCp^*_2$ to BTI-xy in DMA, followed by crystallization using a poor solvent. The crystal structure of **1** was obtained and shown to be trigonal with $CoCp_2^+$, which is shown in Fig. 2a–d.

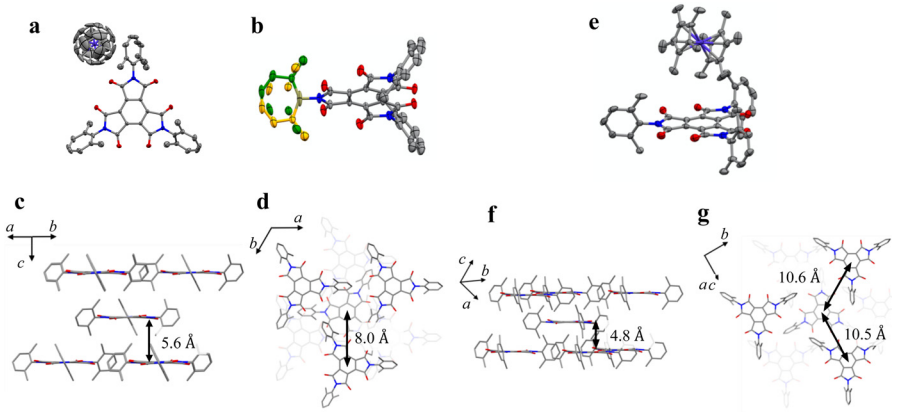

Fig. 2 (a) Crystal structure of **1**. (b) Crystal structure of BTI-xy focused on the disorder of xylene moiety in **1** (yellow and green). (c and d) Perspective view of **1** along the direction parallel to the π-plane of BTI-xy (c), and perpendicular to the π-plane of BTI-xy (d). (e) Crystal structure of **2**. (f and g) Perspective view of **2** along the direction parallel to the π-plane of BTI-xy (f), and perpendicular to the π-plane of BTI-xy (g). The countercations in (c, d, f and g), and hydrogen atoms are omitted for clarity. Purple, Co; red, O; grey, C; and blue, N.

The $CoCp_2^+$ ion is disordered, possibly because it is on the 3-fold helix axis and interacts with the xylene moiety. In fact, structural analysis suggests that the xylene moiety is also disordered (Fig. 2b). In terms of the arrangement of BTI-xy$^{\bullet-}$ in the crystal structure, the vertical distance and the horizontal distance between the centers of BTI-xy$^{\bullet-}$ are estimated to be about 5.6 Å, and about 8.0 Å, respectively (Fig. 2c and d). Considering that the π-stacking interaction generally works at most about 4.0 Å, the π-stacking interaction of BTI-xy$^{\bullet-}$ in **1** should be sufficiently suppressed. On the other hand, the radical anion salt with $CoCp^*_2{}^+$ was crystallized in a monoclinic system with half of BTI-xy$^{\bullet-}$ being crystallographically independent (Fig. 2e–g). Unlike the crystal structure of **1**, the countercation, $CoCp^*_2{}^+$, is not disordered, and the CH–π interactions are observed between the BTI core and hydrogen atom of $CoCp^*_2{}^+$. The vertical distance between the adjacent π-planes of BTI-xy$^{\bullet-}$ is estimated to be about 4.8 Å, and the horizontal distances between the centers of the π-planes are about 10 Å or more, suggesting that the π-stacking interaction is sufficiently suppressed also in **2** (Fig. 2f and g).

Continuous-wave (cw)-ESR

The cw-ESR spectra of **1** and **2** showed isotropic spectral characteristic of $S = 1/2$ spin, and the g-values are the same, $g = 2.0040$, with the line width of 0.93 mT and 0.66 mT, respectively (Fig. 3a and b). Therefore, the electronic structures are expected to be almost the same in both compounds, regardless of the crystal structure. On the other hand, the ESR spectra of **1** and **2** dissolved in DMF/benzene solution showed asymmetric absorption peaks, and these spectra were simulated using $g_{perp} = 2.0044$ and $g_{para} = 2.0017$ for **1** and $g_{perp} = 2.0037$ and $g_{para} = 2.0022$ for **2**, respectively (Fig. 3c and d). These results clearly show that the BTI-xy molecule exists as a radical anion upon the addition of reductants, and that the electron spin in BTI-xy$^{\bullet-}$ is close to the free-electron value ($g = 2.0023$). In spite of the existence of nitrogen atoms in the BTI framework, no hyperfine splitting due to nuclear spins of nitrogen atoms was observed, suggesting that the coupling with nuclear spins is very small. This may be due to the small spin density on the nitrogen atoms (Fig. S2, ESI†).

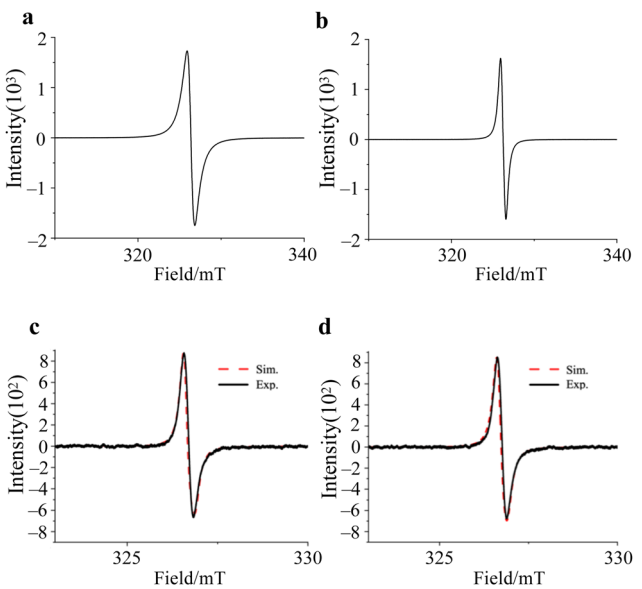

Fig. 3 cw-ESR spectra of crystalline **1** (a) and **2** (b), 0.2 mM DMF/benzene solution of **1** (c) and **2** (d) acquired at RT. Black solid lines and red broken lines are experimental and simulated ESR spectra, respectively.

Magnetic susceptibility

To reveal the spin dynamics of the obtained compounds, dc and ac magnetic susceptibility measurements were performed. The behavior of $\chi_M T$ *vs.* T in each compound follows the Curie law down to around 5 K, with a slight decrease in $\chi_M T$ at lower than 5 K (Fig. S4, ESI†). The decrease in $\chi_M T$ at lower temperature (−20 K) is reproduced using a fitting that considers interactions between spins by the mean-field approximation. The spin–spin interaction in **1** and **2** is assumed to be -0.0635 cm^{-1} and -0.0735 cm^{-1}, respectively, suggesting that BTI-xy$^{\bullet-}$ in **1** and **2** has similar spin–spin interactions. As a result of the crystal structures, the large distance between BTI-xy$^{\bullet-}$ species suppresses the spin–spin interaction in the compounds.

In the ac susceptibility measurement under an applied static magnetic field (B), the susceptibility changes with the applied ac frequency, meaning that the magnetic field-induced relaxation process was successfully measured (Fig. 4 and Fig. S5–S9, ESI†). To the best of our knowledge, this is the first observation of slow magnetic relaxation in organic radicals by ac magnetic susceptibility measurement. The spin–lattice relaxation times (τ) extracted from the fitting with the Cole–Cole plot are discussed below. The measurements were performed on the ground sample and the polycrystalline sample for **1** and **2**, respectively. The τ of polycrystalline **1** is approximately 2.4×10^{-5} s at 2 K (Fig. 4a).

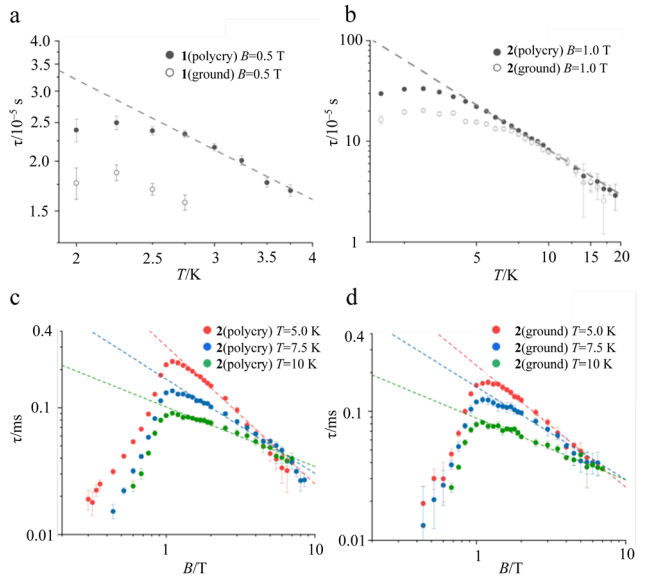

Fig. 4 Temperature dependence of τ in **1** (a), and **2** (b) extracted from ac susceptibility under an applied static magnetic field of 0.5 T, and 1.0 T, respectively. Black dots and open dots represent the τ for the polycrystalline sample and the ground sample, respectively. Magnetic field dependence of τ extracted from ac susceptibility at 5.0 K, 7.5 K, and 10 K for polycrystalline **2** (c) and ground **2** (d). Broken lines are the best fit in the high magnetic field region (≥1.3 T) with $\tau = aB^n$.

Table 1 Fitting parameters of n when the dependence at the high magnetic field is fitted using $\tau = aB^n$

	5.0 K	7.5 K	10 K
Polycrystalline sample (**1**)	−1.09	−0.745	−0.471
Ground sample (**1**)	−0.945	−0.722	−0.481

The relaxation time is almost independent of the temperature up to 2.75 K, and a slow temperature dependence that is proportional to T^{-1} was observed at the higher temperatures. While, **2** exhibits a relaxation time of about 3.0×10^{-4} s at 2 K, which is more than 10 times longer than that of **1** (Fig. 4b). The relaxation time of **2** is almost independent of temperature between 2–5 K, and shows a temperature dependence proportional to $T^{-1.48}$ above 5 K. This temperature dependence is often fitted using the phonon-bottleneck effect,[19] but the relaxation times at high temperatures did not change significantly even in a crushed sample, suggesting that the phonon-bottleneck process is not dominant in the higher temperature range ($T > 7.5$ K). Hence, a different relaxation process from the conventional direct process should exist. We next measured the dependence of the relaxation time on the static magnetic field. While the relaxation time of **1** was short and could not be measured over a wide range of magnetic fields and temperatures, that of **2** could be measured at 5 K, 7.5 K, and 10 K in a wide range of magnetic fields (Fig. 4c and d). The results at 5 K, 7.5 K, and 10 K show that the relaxation times increase with the increasing magnetic field up to about 1 T, and decrease with an increasing magnetic field above 1 T. This tendency is explained by the fact that at low magnetic fields, the internal field due to spin–spin, or spin–nuclear spin interactions is suppressed by the applied magnetic field, while at high magnetic fields, the spin relaxation is enhanced by the Zeeman splitting that corresponds to the energy of the lattice vibration.[21] These behaviors are often fitted with the Brons–van Vleck equation,[20] but in the present data, large deviations from the fitting were observed at high fields, and even the extended Brons–van Bleck equation[11i] cannot follow the data. It is noteworthy that the very slow field dependence at high magnetic fields ($B \geq 1.3$ T) was observed. In Fig. 4c and d, the temperature dependence of τ under high magnetic fields was fitted using $\tau = aB^n$, where a is a pre-exponential factor. The fitting parameters of n are shown in Table 1. Since magnetic relaxations at a high magnetic field are generally promoted by a direct process, it is often fitted as a field dependence of B^{-2}–B^{-4}, but the field dependence is significantly small in this compound. This deviation clearly indicates a non-conventional relaxation process, which was also observed in the temperature dependence of the relaxation time.

Pulsed ESR

Pulsed ESR measurements were performed using the solution-diluted samples in a DMF : benzene = 1 : 1 solvent in order to assess the magnetic relaxation time in an environment without spin–spin interactions. By measuring the echo intensities by the inversion recovery method and the Hahn echo method, we succeeded in obtaining the T_1 and T_2 of the diluted samples. The detailed fitting functions are described in the experimental section. These measurements were recorded up to 50 K, and the results are shown in Fig. 5. Unlike the T_1 measured with ac susceptibility, the T_1 values of **1** and **2** diluted in the solvent showed almost the same trend in the relaxation time. The T_1 values at 10 K and 50 K are 6.5 ms and 27 μs, respectively, showing a sharp decrease in the relaxation time with temperature compared to the crystalline state. The T_1 value at 10 K in the solution-diluted samples is 10 times larger than the τ obtained in the ac susceptibility measurement. The temperature dependencies were reproduced by a phenomenological fitting that takes both the direct and the Raman processes into account;[22]

$$T_1^{-1} = a_{\mathrm{dir}}T + a_{\mathrm{ram}}T^n$$

where a_{dir} and a_{ram} are the coefficients of direct process and Raman process. The contribution of direct and Raman processes to T_1 (Table 2) suggested that the relaxation with the Raman process is dominant above 20 K. In particular, the best fit for **2** was obtained without considering the direct process. The temperature term with the power (n) in the Raman process

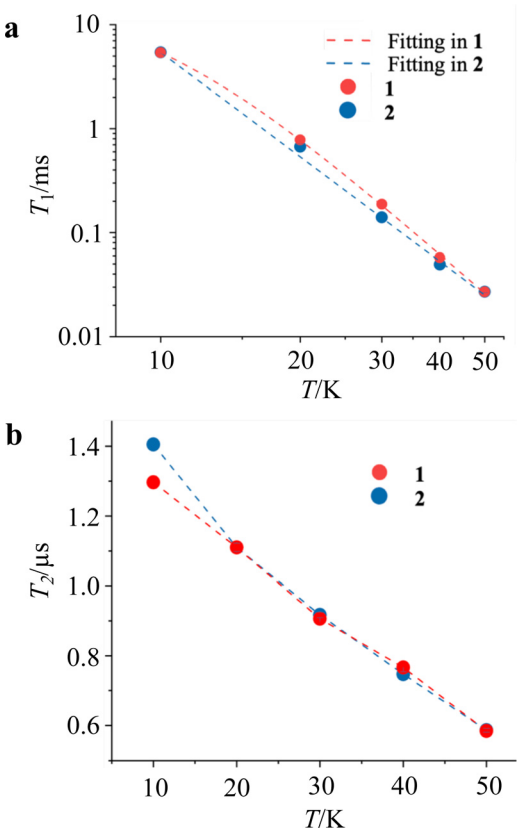

Fig. 5 Temperature dependence of T_1 (a) and T_2 (b) for **1** and **2** in DMF/benzene solution extracted from the pulse echo sequences. Broken lines in (a) and (b) indicate the best-fit models, and a guide for eyes, respectively.

Table 2 Fitting parameters used to fit the temperature dependence of T_1

Sample	a_{dir}	a_{ram}	n
1	0.01135	9.153×10^{-6}	3.893
2	0	8.441×10^{-5}	3.339

is in the range of T^{-3} to T^{-4}, which is often seen in vanadyl complexes.[11g,j,l,p] The phase relaxation times of **1** and **2** are also similar. T_2 shows above 1 μs at 10 K and decreases slowly with increasing temperature, resulting in a phase relaxation time of 0.6 μs at 50 K. Although this phase relaxation time is not the best record for molecular qubits, the relaxation times are of comparable order to those of phthalocyanine and porphyrin complexes with Cu^{2+} and V^{4+} metal ions.[11,12] The relaxation times do not differ significantly depending on the countercation, indicating that the countercation has a little effect on T_2 in this compound.

Discussion

In this study, we have successfully measured the ac magnetic susceptibility and the pulsed ESR measurements of π-organic radical ions by applying the characteristic molecular structure of the BTI-xy molecule, which are unprecedented for the verification of spin dynamics of π-organic radical ions. The cw-ESR measurements for the BTI-xy$^{\bullet-}$ ions show *g*-values which are close to that of the free electron spin (g = 2.0023), indicating the small spin–orbit coupling, which is characteristic of organic radicals. It is important to note that the introduction of xylene has suppressed the π-stacking interactions between radicals and allowed us to measure the relaxation times by ac susceptibility measurement. Here, we have succeeded in observing the spin dynamics of radical molecules in the crystalline state for the first time to the best of our knowledge. In particular, the information on the magnetic relaxation times of **2** is worthy of attention. The characteristic behavior in this experiment is the slow field dependence of the magnetization relaxation time being less than $B^{-1.1}$ in the high field. Such a behavior is much more remarkable than that of other S = 1/2 spins such as Cu^{2+} and V^{4+} where this value is about B^{-2}–B^{-4}, because it enables the application of spins under higher magnetic field and frequency conditions. Since this behavior is also observed in a non-diluted oxovanadyl complex; [VO(TPP)] (TPP = tetraphenylporphyrin), this phenomenon is probably due to the residual spin–spin interaction.[11h] A non-conventional relaxation behavior, meaning a deviation from the direct process, is also observed in the temperature dependence of the relaxation time under 1 T. It is also necessary to mention whether such slow magnetization relaxation is unique to BTI radical systems. Although more extensive research on the magnetic relaxation of π-radical ions is needed, it is noteworthy that the cw-ESR spectra of BTI-xy radicals are not unique but similar to those of other radicals. It indicates that, considering phonons and molecular vibrations separately, π-radical ions isolated from the π-stacking interaction can possess slow magnetic relaxation times. Further research on the generality of π-radical ions in magnetic relaxation will be an important part of the relaxation phenomena in molecular spins.

On the other hand, it is interesting that a large difference in the relaxation time is observed between crystalline **1** and **2**. Since similar *g*-values and spin–spin interactions are obtained from cw-ESR spectra and dc susceptibility measurements, it is unlikely that these factors affect the difference in the relaxation time. Therefore, lattice and molecular vibrations are considered to have a large influence on the relaxation time. This is supported by the fact that T_1 values of **1** and **2** are nearly identical in a diluted solution state. The almost identical absorption spectra in the infrared (IR) region suggest that low-energy vibrational modes are probably the origin of the difference (Fig. S13a, ESI†). Although we do not have information on what specific vibrational modes contribute to the relaxation, the Raman spectra at low energies are significantly different from each other (Fig. S13b, ESI†). The T_2 values longer than 1 μs were observed for **1** and **2** diluted in a DMF : benzene = 1 : 1 solvent at 10 K. This relaxation time, which is comparable to that of metal complexes, may indicate the usefulness of the π-organic radical ions. Interestingly, the difference in T_2 is not observed, even though the $CoCp^*_2{}^+$ molecule contains more hydrogen atoms than $CoCp_2{}^+$. It should be noted that electron spins are generally decohered upon coupling with the neighboring nuclear spins. In fact, in the case of copper complexes, deuteration of the hydrogen atoms in the countercation significantly extends the relaxation time.[11b] The small effect of the countercation may also be due to the covering of the π-plane with the xylene moiety.

Conclusions

In this study, we have performed magnetic measurements on organic radicals, especially on π-organic radical ions by measuring the relaxation behavior. This is the first report of the relaxation behavior of organic radical ions observed by ac susceptibility measurement. We believe that it provides an advanced insight into the possibilities of π-radicals in the study of spin dynamics. In particular, a very slow decrease in the relaxation time under high magnetic fields observed from the magnetic field dependence of the ac susceptibility suggests the possibility to apply the current molecular spin applications at higher magnetic fields and frequencies. The obtained relaxation times are comparable to those of metal complexes that are currently widely studied, and it is an important finding that such results were obtained in spite of the use of xylene, which contains many nuclear spin sources. The present study emphasizes the importance of π-stacking interaction and low-energy molecular vibrations of π-radicals. The ability to study these questions by directly modifying the spin sources of redox-active organic radicals is one of the most attractive features of organic radicals. In addition, we believe this study will motivate further broad research, such as the design of metal–organic frameworks with organic radicals as ligands for scaling of qubits, and a manipulation of quantum states between multiple qubits.

Experimental

Characterization

Elemental analyses were performed with a CHN-S Flash E1112 Thermofinnigan analyzer. ^{1}H NMR measurements were performed on Bruker AV500 of Bruker Japan, Kanagawa, Japan at RT.

Absorption spectra

The solid-state absorption spectra of samples dispersed in 7 mm ϕ KBr pellets were recorded on a FT/IR-4200 spectrometer of JASCO, Tokyo, Japan in the IR region at RT. All samples were prepared in a glovebox and each spectral measurement was performed using a sealed cell. The Raman spectra of samples were recorded on a LabRAM HR Evolution system of Horiba. Polycrystalline samples were excited using a 532 nm laser.

Single-crystal X-ray crystallography

Single-crystal X-ray diffraction measurements for samples were performed on a XtaLAB AFC10 diffractometer with a HyPix-6000HE hybrid pixel array detector, graphite monochromated Mo Kα radiation (λ = 0.7107 Å), and a cryogenic equipment GN-2D/S of Rigaku, Tokyo, Japan. The temperature was set by blowing chilled nitrogen flow. The crystal structure was solved using direct methods (SHELXT) followed by Fourier synthesis. Structure refinement was performed using full-matrix least-squares procedures with SHELXL on F^2, where F is the crystal structure factor, in the Olex2 software.[23] All non-H atoms were refined with anisotropic displacement parameters. Graphical material was prepared using Mercury CSD 4.2 software (copyright CCDC, https://www.ccdc.cam.ac.uk/mercury/)

Magnetic measurements

Magnetic susceptibility measurements were performed on Quantum Design SQUID magnetometers MPMS-XL, PPMS VSM system. Direct current (dc) measurements were performed in the range of 1.8–300 K in a dc magnetic field of 1000 Oe. Randomly oriented fresh polycrystalline samples were used for the measurements. The diamagnetic contributions of the samples and sample holder were estimated by using Pascal's constants.[24] The fitting of the $\chi_M T$ *vs.* T plot were performed using PHI software.[25] Temperature-dependent alternate current (ac) susceptibility measurements of **CoCp$_2$BTI-xy** (**1**) and **CoCp*$_2$BTI-xy** (**2**) were performed in the frequency (ν) range of 10–10 000 Hz by applying an oscillating field of 3 Oe in the temperature range of 2.0–5.0 K and 2.0–20 K, respectively. A static magnetic field up to 8.5 T was applied. The results of the frequency-dependent ac susceptibility were fitted using the Cole–Cole plot, which is presented below. The fitting of the results was performed using least-squares procedures.

$$\chi' = \chi_S + (\chi_T - \chi_S)\frac{(2\pi\nu\tau)^{1-\alpha}\sin\left(\frac{\pi\alpha}{2}\right)}{1 + 2(2\pi\nu\tau)^{1-\alpha}\sin\left(\frac{\pi\alpha}{2}\right) + (2\pi\nu\tau)^{2-2\alpha}}$$

$$\chi'' = (\chi_T - \chi_S)\frac{(2\pi\nu\tau)^{1-\alpha}\cos\left(\frac{\pi\alpha}{2}\right)}{1 + 2(2\pi\nu\tau)^{1-\alpha}\sin\left(\frac{\pi\alpha}{2}\right) + (2\pi\nu\tau)^{2-2\alpha}}$$

Calculation methods

Quantum chemistry calculations were performed using the density functional theory (DFT) calculation method. The gaussian16 package was used for the calculation of spin density.[26] For the exchange–correlation functional and basis set system, B3LYP/6-311+(G) was applied.[27]

Electron spin resonance

cw-X-band (frequency ≈ 9.163 GHz) ESR spectra of the samples were recorded on a JEOL, X330 spectrometer. The samples were sealed in quartz glass to prevent them from coming in contact with air or water. The spectra of polycrystalline samples were measured with the following parameters, temperature: 293 K, modulation width: 0.1 mT, power: 1 mW, time constant: 0.03 s. The simulation and fitting of the EPR spectra were performed with AniSimu/FA ver.2.4.0 from JEOL RESONANCE inc. Pulsed ESR spectra were observed on a Bruler ESP380E ESR spectrometer with a continuous flow helium cryostat. The spectrometer was fully controlled using SpecMan4EPR software.[28] Phase memory times were measured using the Hahn echo sequence (π/2–τ–π–τ–echo) with increasing τ from 0.5 μs to 4.5 μs with a pulse length of $t_{\pi/2}$ = 100 ns and t_π = 200 ns. Spin–lattice relaxation times were measured using the standard inversion recovery sequence (π–t_d–π/2–τ–π–τ–echo) with the pulse length of $t_{\pi/2}$ = 100 ns and t_π = 200 ns. The change in the intensity of two pulse echoes (π/2–τ–π–τ–echo) and three pulse echoes (π–t_d–π/2–τ–π–τ–echo) with the length of t_d and τ are fitted using the following equation;

$$I = I_m + k_m \exp(-2\tau/T_2)\, I = I_1 + k_1 \exp(-t_d/T_1)$$

where I indicates the echo intensity, and I_m, k_m, I_1, and k_1 indicate coefficients.

Synthetic procedures

***N*-(2,6-Dimethylphenyl)maleimide.** 2,6-Dimethylaniline 24.2 g (200 mmol) in 100 mL ether was added to maleic anhydride 19.6 g (200 mmol) in 200 mL of ether for 5 min with stirring at 0 °C. After 1 h of stirring, the precipitated white solids were collected and dried *in vacuo*. 100 mL of Ac_2O was poured into the obtained white solid and AcONa 16.4 g (200 mmol), and then refluxed at 90 °C for 30 min. After cooling to RT, 300 mL of H_2O was added to the solution and stirred for 2 h. 300 mL of ether was added to the suspension after stirring and the organic layer was separated. This organic layer was washed with brine twice, dried with $MgSO_4$, and evaporated using a rotary evaporator. The resulting white solid was washed with water and vacuum-dried to give 28.9 g of the desired compound. Yield: 71.8% ^{1}H NMR (500 MHz, DMSO, 298 K, ppm) δ 7.28(t, 1H), 7.25(s, 2H), 7.19(d, 2H), 2.04(s, 6H).

2-Bromo-*N*-(2,6-dimethylphenyl)maleimide. Bromine 9.59 g (60 mmol) in 15 mL of CH_2Cl_2 was added dropwise to *N*-(2,6-dimethylphenyl)maleimide 10.05 g (50 mmol) in 100 mL of CH_2Cl_2 for 10 min. After refluxing this solution at 55 °C for 1 h, a pale brown solid was obtained by evaporating the solution. 100 mL of tetrahydrofuran (THF) was poured into the solid and cooled on ice. To the solution, 5.05 g (50 mmol) of triethylamine dissolved in 10 mL of tetrahydrofuran was added dropwise. The precipitated white solid after 2 h stirring was filtered, and the filtrate was evaporated to obtain the desired yellow oily substance. In this reaction, the product was not purified and used in the next reaction.

2-Dimethylamino-*N*-(2,6-dimethylphenyl)maleimide. 50 wt% aqueous $NHMe_2$ solution 4.50 g (50 mmol) in 10 mL of THF and triethylamine 6.06 g (60 mmol) in 10 mL of THF were added into the obtained 2-bromo-*N*-(2,6-dimethylphenyl)maleimide which was dissolved into 100 mL of THF with stirring at RT. After stirring for 1 h, the resulting suspension was filtered and the filtration was evaporated to obtain a yellow crystalline solid. This yellow solid was washed with H_2O and dried to give 5.5 g of 2-dimethylamino-*N*-(2,6-dimethylphenyl)maleimide. Yield: 45.0% (the yield from *N*-(2,6-dimethylphenyl)maleimide) ^{1}H NMR (500 MHz, DMSO, 298 K, ppm) δ 7.24(t, 1H), 7.16(s, 2H), 5.15(s, 1H), 3.10(br, 6H), 2.04(s, 6H).

***N*,*N*′,*N*″-Tris(2,6-dimethylphenyl)benzenetriimide.** 2-Dimethylamino-*N*-(2,6-dimethylphenyl)maleimide 3.0 g (12.3 mmol) in AcOH : H_2O = 4 : 1 (v/v) 18 mL was refluxed at 80 °C for 30 min without stirring. After just heating, the resulting dark brown solution was stirred with additional 30 min reflux. With additional heating and stirring, a pale yellow solid precipitated in the solution. After cooling to room temperature, the precipitated pale yellow solid was filtered, washed with water, and dried *in vacuo*. The crude sample was purified through column chromatography with $CHCl_3$: MeOH = 19 : 1. To obtain the crystals of BTI-xy, thermal recrystallization with toluene was performed, resulting in yellow crystals of BTI-xy$^\bullet$ toluene 640 mg. Yield: 26.1% ^{1}H NMR (500 MHz, DMSO, 298 K, ppm) δ 7.38(t, 1H), 7.29(d, 2H), 2.18(s, 6H) Anal. calcd for $C_{43}H_{35}N_3O_6$: C, 74.88; H, 5.11; N, 6.03. Found: C, 74.97; H, 5.09; N, 6.05.

CoCp2BTI-xy (1). $CoCp_2$ 21.3 mg (11.2 μmol) and BTI-xy$^\bullet$ toluene 51.7 mg (7.5 μmol) were dissolved into 4.5 mL of dimethylacetamide (DMA). This green solution was put into grass tubes and diffused with diethy lether at room temperature for 5 days. Dark green crystals of **1** were obtained from the solution. Anal. calcd for $C_{46}H_{37}CoN_3O_6$: C, 70.23; H, 4.74; N, 5.34. Found: C, 69.94; H, 4.87; N, 5.31.

CoCp*$_2$BTI-xy (2). $CoCp^*_2$ 16.5 mg (5.0 μmol) and BTI-xy$^\bullet$ toluene 34.5 mg (5.0 μmol) were dissolved into 5 mL of DMA. This green solution was put into grass tubes and diffused with diethyl ether at room temperature for 2 days. Dark green crystals of **2** were obtained from the solution. Anal. calcd for $C_{56}H_{57}CoN_3O_6$: C, 72.56; H, 6.20; N, 4.53. Found: C, 71.56; H, 6.39; N, 4.75.

Author contributions

S. K. conceived and designed the project, carried out the synthesis, characterization, crystal structure analysis, measurements of magnetic properties, and wrote the manuscript. K. S. contributed to the pulsed ESR measurements. M. Y., R. S., and H. I. provided resources and contributed to the project administration.

Conflicts of interest

There are no conflicts to declare.

Acknowledgements

This work was supported by JSPS KAKENHI grant numbers JP20J22404 (S. K.), JP21H01901 (H. I.), JP21K18971 (H. I.), JP19H05631 (M. Y.), JP20H02547 (R. S.), JP18KK0395 (R. S.), and JP19H05621 (K. S.), by the Toyota Riken Scholar Program (H. I.), by the Iketani Science and Technology Foundation 0331101-A (H. I.), by The Murata Science Foundation (H. I.) and by the National Natural Science Foundation of China (NSFC, 22150710513). M. Y. acknowledges the support of the 111 project (B18030) from China.

Notes and references

1 (*a*) M. A. Nielsen and I. L. Chuang, *Quantum Computation and Quantum Information; 10th anniversary edition*, Cambridge University Press, Cambridge, 2010; (*b*) T. D. Ladd, F. Jelezko, R. Laflamme, Y. Nakamura, C. Monroe and J. L. O'Brien, *Nature*, 2010, **464**, 45–53.

2 (*a*) Y. Wu, F. Jelezko, M. B. Plenio and T. Weil, *Angew. Chem., Int. Ed.*, 2016, **55**, 6586–6598; (*b*) C.-J. Yu, S. von Kugelgen, D. W. Laorenza and D. E. Freedman, *ACS Cent. Sci.*, 2021, **7**, 712–723; (*c*) S. E. Crawford, R. A. Shurayev, H. P. Paudel, P. Lu, M. Syamlal, P. R. Ohodnicki, B. Chorpening, R. Gentry and Y. Duan, *Adv. Quantum Technol.*, 2021, **4**, 2100049.

3 E. Knill, R. Laflamme and G. J. Milburn, *Nature*, 2001, **409**, 46–52.

4 D. J. Wineland, C. Monroe, W. N. Itano, D. Leibfried, B. E. King and D. M. Meekhof, *J. Res. Natl. Inst. Stand. Technol.*, 1998, **103**, 259–328.

5 (*a*) N. A. Gershenfeld and I. L. Chuang, *Science*, 1997, **275**, 350–356; (*b*) D. G. Cory, A. F. Fahmy and T. F. Havel, *Proc. Natl. Acad. Sci. U. S. A.*, 1997, **94**, 1634–1639.

6 (*a*) Y. Nakamura, Y. A. Pashkin and J. S. Tsai, *Nature*, 1999, **398**, 786–788; (*b*) D. Vion, A. Aassime, A. Cottet, P. Joyez, H. Pothier, C. Urbina, D. Esteve and M. H. Devoret, *Science*, 2000, **296**, 886–889.

7 (*a*) A. Gaita-Ariño, F. Luis, S. Hill and E. Coronado, *Nat. Chem.*, 2019, **11**, 301–309; (*b*) M. Atzori and R. Sessoli, *J. Am. Chem. Soc.*, 2019, **141**, 11339–11352.

8 X. Zhang, C. Wolf, Y. Wang, H. Aubin, T. Bilgeri, P. Willke, A. J. Heinrich and T. Choi, *Nat. Chem.*, 2022, **14**, 59–65.

9 (*a*) G. Aromí, D. Aguilá, P. Gamez, F. Luis and O. Roubeau, *Chem. Soc. Rev.*, 2012, **41**, 537–546; (*b*) F. Troiani and M. Affronte, *Chem. Soc. Rev.*, 2011, **40**, 3119.

10 (*a*) A. Ardavan, O. Rival, J. J. Morton, S. J. Blundel, A. M. Tyryshkin, G. A. Timco and R. E. P. Winpenny, *Phys. Rev. Lett.*, 2007, **98**, 057201; (*b*) J. Ferrando-Soria, E. M. Pineda, A. Chiesa, A. Fernandez, S. A. Magee, S. Carrerra, P. Santini, I. J. Vitorica-Yrezabal, F. Tuna, G. A. Timco, E. J. L. Mclnnes and R. E. P. Winpenny, *Nat. Commun.*, 2016, **7**, 11377; (*c*) A. Ardavan, A. M. Bowen, A. Fernandez, A. Fielding, D. Kaminski, F. Moro, C. A. Muryn, M. D. Wise, A. Ruggi, E. J. L. Mclnnes, K. Severin, G. A. Timco, C. R. Timmel, F. Tuna, G. F. S. Whitehead and R. E. P. Winpenny, *npj Quantum Inf.*, 2015, **1**, 15012; (*d*) A. Fernandez, J. Ferrando-Soria, E. M. Pineda, F. Tuna, I. J. Vitorica-Yrezabal, C. Knappe, J. Ujma, C. A. Muryn, G. A. Timco, P. E. Barran, A. Ardavan and R. E. P. Winpenny, *Nat. Commun.*, 2016, **7**, 10240; (*e*) S. Bertaina, S. Gambarelli,

T. Mitra, B. Tsukerblat, A. Müller and B. Barbala, *Nature*, 2008, **453**, 203–207.

11 (*a*) J. M. Zadrozny, J. Niklas, O. G. Poluektov and D. E. Freedman, *J. Am. Chem. Soc.*, 2014, **136**, 15841–15844; (*b*) J. M. Zadrozny, J. Niklas, O. G. Poluektov and D. E. Freedman, *ACS Cent. Sci.*, 2015, **1**, 488–492; (*c*) C.-J. Yu, M. J. Graham, J. M. Zadrozny, J. Niklas, M. D. Krzyaniak, M. R. Wasielewski, O. G. Poluektov and D. E. Freedman, *J. Am. Chem. Soc.*, 2016, **138**, 14678–14685; (*d*) M. J. Graham, C.-J. Yu, M. D. Krzyaniak, M. R. Wasielewski and D. E. Freedman, *J. Am. Chem. Soc.*, 2017, **139**, 3196–3201; (*e*) M. J. Graham, M. D. Krzyaniak, M. R. Wasielewski and D. E. Freedman, *Inorg. Chem.*, 2017, **56**, 8106–8113; (*f*) M. Atzori, L. Tesi, E. Morra, M. Chiesa, L. Sorace and R. Sessoli, *J. Am. Chem. Soc.*, 2016, **138**, 2154–2157; (*g*) M. Atzori, E. Morra, L. Tesi, A. Albino, M. Chiesa, L. Sorace and R. Sessoli, *J. Am. Chem. Soc.*, 2016, **138**, 11234–11244; (*h*) T. Yamabayashi, M. Atzori, L. Tesi, G. Cosquer, F. Santanni, M.-E. Boulon, E. Morra, R. Torre, M. Chiesa, L. Sorace, R. Sessoli and M. Yamashita, *J. Am. Chem. Soc.*, 2018, **140**, 12090–12101; (*i*) M. Atzori, L. Tesi, S. Benci, A. Lunghi, R. Righini, A. Taschin, R. Torre, L. Sorace and R. Sessoli, *J. Am. Chem. Soc.*, 2017, **139**, 4338–4341; (*j*) M. Atzori, S. Benci, E. Morra, L. Tesi, M. Chiesa, R. Torre, L. Sorace and R. Sessoli, *Inorg. Chem.*, 2018, **57**, 731–740; (*k*) L. Tesi, E. Lucaccini, I. Cimatti, M. Perfetti, M. Mannini, M. Atzori, E. Morra, M. Chiesa, A. Caneschi, L. Sorace and R. Sessoli, *Chem. Sci.*, 2016, **7**, 2074–2083; (*l*) L. Tesi, A. Lunghi, M. Atzori, E. Lucaccini, L. Sorace, F. Totti and R. Sessoli, *Dalton Trans.*, 2016, **45**, 16635; (*m*) E. Garlatti, L. Tesi, A. Lunghi, M. Atzori, D. J. Voneshen, P. Santini, S. Sanvito, T. Guidi, R. Sessoli and S. Carretta, *Nat. Commun.*, 2020, **11**, 1751; (*n*) A. Albino, S. Benci, M. Atzori, L. Chelazzi, S. Ciattini, A. Taschin, P. Bartolini, A. Lunghi, R. Righini, R. Torre, F. Totti and R. Sessoli, *J. Phys. Chem. C*, 2021, **125**, 22100–22110; (*o*) A. Albino, S. Benci, L. Tesi, M. Atzori, R. Totti, S. Sanvito, R. Sessoli and A. Lunghi, *Inorg. Chem.*, 2019, **58**, 10260–10268; (*p*) M. S. Fataftah, M. D. Krzyaniak, B. Vlaisavljevich, M. R. Wasielewski, J. M. Zadrozny and D. E. Freedman, *Chem. Sci.*, 2019, **10**, 6707–6714.

12 (*a*) K. Bader, M. Winkler and J. van Slageren, *Chem. Commun.*, 2016, **52**, 3623–3626; (*b*) A. H. Follmer, R. D. Ribson, P. H. Oyala, G. Y. Chen and R. G. Hadt, *J. Phys. Chem. A*, 2020, **124**, 9252–9260; (*c*) R. Mirzoyan and R. G. Hadt, *Phys. Chem. Chem. Phys.*, 2020, **22**, 11249–11265; (*d*) N. P. Kazmierczak, R. Mirzoyan and R. G. Hadt, *J. Am. Chem. Soc.*, 2021, **143**, 17305–17315; (*e*) K. Bader, D. Dengler, S. Lenz, B. Endeward, S.-D. Jiang, P. Neugebauer and J. van Slageren, *Nat. Commun.*, 2014, **5**, 5304; (*f*) C.-J. Yu, S. von Kugelgen, M. D. Krzyaniak, W. Ji, W. R. Dichtel, M. R. Wasielewski and D. E. Freedman, *Chem. Mater.*, 2020, **32**, 10200–10206; (*g*) F. Santanni, A. Albino, M. Atzori, D. Ranieri, E. Salvadori, M. Chiesa, A. Lunghi, A. Benci, L. Sorace, F. Totti and R. Sessoli, *Inorg. Chem.*, 2021, **60**, 140–151; (*h*) M. Warner, S. Din, I. S. Tupitsyn, G. W. Morley, A. M. Stoneham, J. A. Gardener, Z. Wu, A. J. Fisher and S. Heutz, *Nature*, 2013, **503**, 504–509.

13 (*a*) R. Owenius, G. R. Eaton and S. S. Eaton, *J. Magn. Reson.*, 2005, **172**, 168–175; (*b*) Y. Shou, B. E. Bowler, G. R. Eaton and S. S. Eaton, *J. Magn. Reson.*, 1999, **139**, 165–174; (*c*) R. Owenius, G. E. Terry, M. J. Williams, S. S. Eaton and G. R. Eaton, *J. Phys. Chem. B*, 2004, **108**, 9475–9481; (*d*) A. Ueda, S. Suzuki, K. Yoshida, K. Fukui, K. Sato, T. Takui, K. Nakasuji and Y. Morita, *Angew. Chem., Int. Ed.*, 2013, **52**, 4795–4799; (*e*) A. A. Kuzhelev, D. V. Trukhin, O. A. Krumkacheva, R. K. Strizhakov, O. Y. Rogozhnikova, T. I. Troitskaya, M. V. Fedin, V. M. Tormyshev and E. G. Bagryanskaya, *J. Phys. Chem. B*, 2015, **119**, 13630–13640; (*f*) R. M. Jacobberger, Y. Qiu, M. L. Williams, M. D. Krzyaniak and M. R. Wasielewski, *J. Am. Chem. Soc.*, 2022, **144**, 2276–2283; (*g*) S. Nakazawa, S. Nishida, T. Ise, T. Yoshino, N. Mori, R. D. Rahimi, K. Sato, Y. Morita, K. Toyota, D. Shiomi, M. Kitagawa, H. Hara, P. Carl, P. Höfer and T. Takui, *Angew. Chem., Int. Ed.*, 2012, **51**, 9860–9864; (*h*) F. Lombardi, A. Lodi, J. Ma, J. Liu, M. Slota, A. Narita, W. K. Myers, K. Müllen, X. Feng and L. Bogani, *Science*, 2019, **366**, 1107–1110; (*i*) M. Slota, A. Keerthi, W. K. Myers, E. Tretyakov, M. Baumgarten, A. Ardavan, H. Sadeghi, C. J. Lambert, A. Narita, K. Müllen and L. Bogani, *Nature*, 2018, **557**, 691–696; (*j*) R. M. Brown, Y. Ito, J. H. Warner, A. Ardavan, H. Shinohara, A. D. Briggs and J. J. L. Morton, *Phys. Rev. B: Condens. Matter Mater. Phys.*, 2010, **82**, 033410; (*k*) Z. Liu, B.-W. Dong, H.-B. Meng, M.-X. Xu, T.-S. Wang, B.-W. Wang, C.-R. Wang, S.-D. Jiang and S. Gao, *Chem. Sci.*, 2018, **9**, 457–462; (*l*) A. S. Poryvaev, E. Gjuzi, D. M. Polyukhov, F. Hoffmann, M. Fröba and M. V. Fedin, *Angew. Chem., Int. Ed.*, 2021, **60**, 8683–8688; (*m*) Y.-Z. Dai, B.-W. Dong, Y. Kao, Z.-Y. Wang, H.-L. Un, Z. Liu, Z.-J. Lin, L. Li, F.-B. Xie, Y. Lu, M.-X. Xu, T. Lei, Y.-J. Sun, J.-Y. Wang, S. Gao, S.-D. Jiang and J. Pei, *ChemPhysChem*, 2018, **19**, 2972–2977.

14 (*a*) Y. Lin, Y. Li and X. Zhan, *Chem. Soc. Rev.*, 2012, **41**, 4245–4272; (*b*) T. Mori, *Chem. Rev.*, 2004, **104**, 4947–4970.

15 (*a*) N. J. Tao, *Phys. Rev. Lett.*, 1996, **76**, 4066–4069; (*b*) I. V. Pobelov, Z. Li and T. Wandlowski, *J. Am. Chem. Soc.*, 2008, **130**, 16045–16054.

16 M. J. Graham, J. M. Zadrozny, M. S. Fataftah and D. E. Freedman, *Chem. Mater.*, 2017, **29**, 1885–1897.

17 (*a*) D.-H. Tuo, C. Chen, H. Ruan, Q.-Q. Wang, Y.-F. Ao, X. Wang and D.-X. Wang, *Angew. Chem., Int. Ed.*, 2020, **59**, 14040–14043; (*b*) S. Koyama, Y. Horii, T. Sato, S. Takaishi, N. Hoshino, T. Akutagawa and H. Iguchi, *ChemPhysChem*, 2022, e202200322; (*c*) D.-H. Tuo, S. Tang, P. Jin, J. Li, X. Wang, C. Zhang, Y.-F. Ao, Q.-Q. Wang and D.-X. Wang, *CCS Chem.*, 2022, DOI: 10.31635/ccschem.022.202202167.

18 (*a*) D.-H. Tuo, Q. He, Q.-Q. Wang, Y.-F. Ao and D.-X. Wang, *Chin. J. Chem.*, 2019, **37**, 684–688; (*b*) K. A. McMenimen and D. G. Hamilton, *J. Am. Chem. Soc.*, 2001, **123**, 6453–6454.

19 N. G. Connelly and W. E. Geiger, *Chem. Rev.*, 1996, **96**, 877–910.

20 J. H. Van Vleck, *Phys. Rev.*, 1941, **59**, 724–729.

21 S. Gomez-Coca, A. Urtizberea, E. Cremades, P. J. Alonso, A. Camoń, E. Ruiz and F. Luis, *Nat. Commun.*, 2014, **5**, 4300.

22 K. J. Standley and R. A. Vaughan, *Electron Spin Relaxation Phenomena in Solids*, Springer US, Boston, MA, 1969.
23 (*a*) G. M. Sheldrick, *Acta Crystallogr., Sect. C: Struct. Chem.*, 2015, **C71**, 3–8; (*b*) G. M. Sheldrick, *Acta Crystallogr., Sect. A: Found. Adv.*, 2015, **71**, 3–8; (*c*) O. V. Dolomanov, L. J. Bourhis, R. J. Gildea, J. A. K. Howard and H. Puschmann, *J. Appl. Crystallogr.*, 2009, **42**, 339–341.
24 G. A. Bain and J. F. Berry, *J. Chem. Educ.*, 2008, **85**, 532–536.
25 N. F. Chilton, R. P. Anderson, L. D. Turner, A. Soncini and K. S. Murray, *J. Comput. Chem.*, 2013, **34**, 1164–1175.
26 *Gaussian 16, Revision C.01*, Gaussian, Inc., Wallingford, CT, USA, 2016.
27 (*a*) A. D. Becke, *J. Chem. Phys.*, 1993, **98**, 1372–1377; (*b*) C. Lee, W. Yang and R. G. Parr, *Phys. Rev. B: Condens. Matter Mater. Phys.*, 1988, **37**, 785–789.
28 B. Epel, I. Gromov, S. Stoll, A. Schweiger and D. Goldfarb, *Concepts Magn. Reson., Part B*, 2005, **26B**, 36–45.